Structural Performance of Confined Masonry Walls Retrofitted Using Ferrocement and GFRP under In-Plane Cyclic Loading

ARTICLE *in* ENGINEERING STRUCTURES · APRIL 2015

Impact Factor: 1.84

4 AUTHORS, INCLUDING:

Osama Ahmed Kamal

Benha University

30 PUBLICATIONS **137** CITATIONS

SEE PROFILE

Engineering Structures 94 (2015) 54–69

Contents lists available at ScienceDirect

Engineering Structures

journal homepage: www.elsevier.com/locate/engstruct

Structural performance of confined masonry walls retrofitted using ferrocement and GFRP under in-plane cyclic loading

Mosaad El-Diasity [a,*], Hussein Okail [b], Osama Kamal [a], Mohamed Said [a]

[a] Structural Engineering Department, Shoubra Faculty of Engineering, Benha University, Egypt
[b] Structural Engineering Department, Ain Shams University, Egypt

ARTICLE INFO

Article history:
Received 2 May 2014
Revised 13 March 2015
Accepted 14 March 2015

Keywords:
Confined masonry
Seismic behavior
Cyclic loading
Shear failure
Ferrocement
Expanded mesh
Glass woven fibers

ABSTRACT

This paper presents the results of in-plane cyclic loading tests conducted on confined masonry walls retrofitted using low-cost ferrocement and GFRP systems. Ten wall assemblies with a 0.80-scale were built, consisting of a clay masonry panel, two confining columns and a tie beam. The assemblies were tested under a combination of a vertical load and lateral reversed cyclic loading with a displacement controlled loading protocol up to failure. Wall panels had various configurations, namely, solid walls, perforated walls with window and door openings. Two composite materials (ferrocement and GFRP) and three retrofitting configurations (diagonal "X", corner, and full coverage) were investigated. Key experimental results showed that the proposed upgrading techniques improved the lateral resistance of the confined walls by a factor ranging from 25% to 32%with a significant increase in the ductility and energy absorption of the panel ranging from 33% to 85%; however, the improvement in lateral drifts was less significant. Regarding the upgrading configurations, the diagonal "X" and full coverage can help prevent diagonal shear failure especially in tie columns and convert the failure mode to a panel-rocking mode. Additionally, in all retrofitting cases, collapse was significantly delayed by maintaining the wall integrity under large lateral deformations. A good agreement was found by comparing deformed shapes, crack patterns and capacity curves of finite element models included in this study.

1. Background information

Confined masonry construction has emerged as a building technology that offers an alternative to both unreinforced masonry and infilled reinforced concrete (RC) frame construction. The system consists of masonry panel confined with horizontal and vertical RC elements with light reinforcement ratio. The confined masonry is considerably different from infilled RC frame with respect to its construction methodology, as the masonry wall is laid before the tie columns (Brzev [1]). The system also differs by the load transfer mechanism under gravity and lateral load, the masonry wall transmit the gravity load from the slab above down to the foundation. The walls act as bracing panels; confining elements (tie column and tie beam) provide restraint to masonry panel and protect it from complete disintegration especially under large lateral deformations (Yoshimura et al. [2]).

The in-plane response of a confined masonry wall is distinctly different from that of reinforced concrete infilled frames. Although the confined masonry wall experiences both flexural and shearing deformations, the masonry infill deforms in a shear mode within a frame that attempts to deform in flexure, resulting in separation of the frame and infill wall along the tension diagonal (Riahi et al. [3]).

As a result, improvement in deformation and energy dissipation characteristics are also achieved if the system is properly constructed (Tomazevic and Klemenc [4]).

A confined masonry wall subjected to in-plane lateral earthquake loading develops either a shear or flexural failure mechanisms (Tomazevic and Klemenc [4]; Yoshimura et al. [2]). Shear failure mechanism is characterized by distributed diagonal cracking in the wall. The damage is caused either by the bond destruction at the mortar–brick interface (shear-friction mechanism), or tensile cracking in the masonry units (Tomazevic [5]). Flexural failure mechanism due to in-plane lateral loads is characterized by horizontal cracking of the bed-joints located on the tension side of the wall (Yoshimura et al. [2]). Separation of the tie-columns from the wall was observed in some cases when a toothed wall-to-column connection was absent, and there were no connecting ties between the tie-column and the wall. Flexural mechanism is not as critical as shear mechanism since it does not lead to brittle

* Corresponding author.
E-mail address: ec_cai_mosaad.hassan@yahoo.com (M. El-Diasity).

http://dx.doi.org/10.1016/j.engstruct.2015.03.035
0141-0296/

Table 1
Design summary of tested walls.

Wall ID	Wall state	Masonry panel	Retrofitting configuration	Long RFT	Trans RFT	Vertical stress (MPa)
Un-retrofitted						
CLY-S-CTRL	Unretrofitted	Solid	–	4T10	T6@20 cm	0.5
CLY-P-W	Unretrofitted	Perforated window	–	4T10	T6@20 cm	0.5
CLT-P-D	Unretrofitted	Perforated door	–	4T10	T6@20 cm	0.5
Retrofitted						
CLY-D-FERRO	Retrofitted	Door perforated	Ferrocement full coverage	4T10	T6@20 cm	0.5
CLY-W-FERRO	Retrofitted	Perforated window	Ferrocement full coverage	4T10	T6@20 cm	0.5
CLY-S-FERRO-C	Retrofitted	Solid	Ferrocement connections	4T10	T6@20 cm	0.5
CLY-S-FERRO-X	Retrofitted	Solid	Ferrocement X-diagonal	4T10	T6@20 cm	0.5
CLY-S-FERRO-F	Retrofitted	Solid	Ferrocement full coverage	4T10	T6@20 cm	0.5
CLY-S-GFRP-X	Retrofitted	Solid	GFRP X-diagonal	4T10	T6@20 cm	0.5
CLY-S-GFRP-F	Retrofitted	Solid	GFRP full coverage	4T10	T6@20 cm	1.0

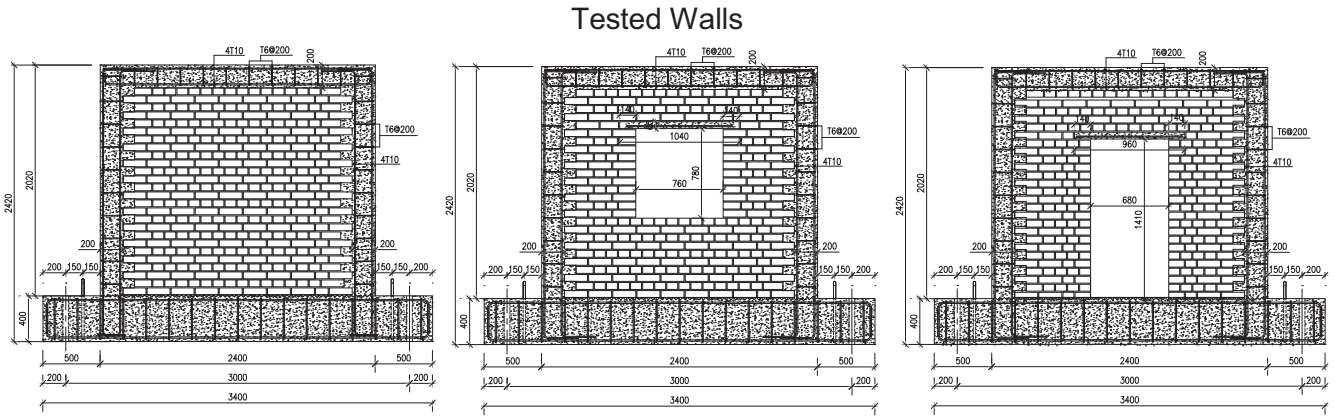

Fig. 1. Typical details of the tested walls assemblies.

(a) Footing with column reinforcement (b) Masonry wall construction

(c) Concrete casting of tie column (d) Concrete casting of tie Beam

Fig. 2. Construction sequence of a typical wall assembly.

(a) Spatter-dashing of wall (b) Fixing the expanded Mesh (c) Laying of mortar layer

Fig. 3. Procedures of retrofitting walls by ferrocement.

Table 2
Properties of the GFRP material.

Commercial name	Weight	Breaking Strength	Fiber diameter (μm)
EWR-600	600 g/m^2	3850 N/50 mm	13

failure, although crushing and disintegration of masonry in the compression toe area of the wall may take place (Tomazevic [5]).

Moreover, during an earthquake, the masonry panels are subjected to in-plane and out-of-plane loads simultaneously. The out-of-plane load-carrying capacity of these masonry panels may be substantially weakened after being damaged, endangering their overall safety and stability. The extent of damage and likelihood of wall collapse in the out-of-plane direction also depends on the type of floor diaphragm (rigid or flexible), the spacing between confining elements, and the connection of masonry panel with adjacent confining elements. Good bonding between the masonry wall and adjacent RC tie-columns is essential for satisfactory earthquake performance, and for delaying undesirable cracking and separation of wall with confining elements. The shake table test on confined masonry walls conducted by Tu et al. [6] concluded that the strong boundary connection prevent masonry panel from falling out of the frame and thus can sustain considerable out-of-plane seismic loads.

Opening size and the degree of coupling affect both initial stiffness and cracking pattern. The rate, at which stiffness degrades, however, is almost independent of these factors (Ishibashi et al. [7]). While excessively large openings could reduce shear capacity of confined masonry walls by almost 50% (Gostic and Zarnic [8]), their effect on seismic performance is almost negligible when size is restrained to approximately 10% of the wall gross area (Yanez et al. [9]).

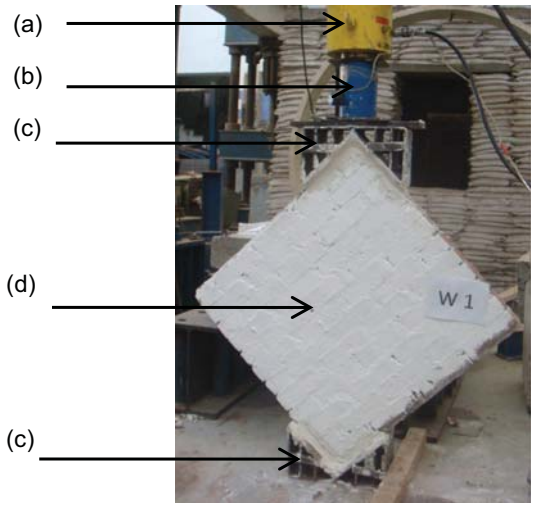

Fig. 5. Test set up of diagonal compression test.

A prediction method on structural performance for confined masonry walls and for retrofitting of confined masonry walls were presented by Lourdes Ana et al. [10] with comparison of results of structural test performed at structural laboratory in CISMID UNI-Lima-Peru. The cyclic loading tests on walls were carried out two different kinds of the retrofitted schemes of confined masonry walls: the one was a wire mesh wrapping alternative and the other was the combined materials such as adhesive and disposal mats with different arrangements. The methodology to evaluate structural performance for retrofitted confined masonry wall was

(a) Laying of thin layer of mortar (b) Painting polyester risen (c) Laying of GFRP sheets

Fig. 4. Procedures of retrofitting walls by GFRP.

a – Hydraulic jack; b – Load cell; c – Loading shoes; d – Masonry specimen

(a) Wallet W1 (b) Wallet W2

Fig. 6. Failure patterns of the tested wallets.

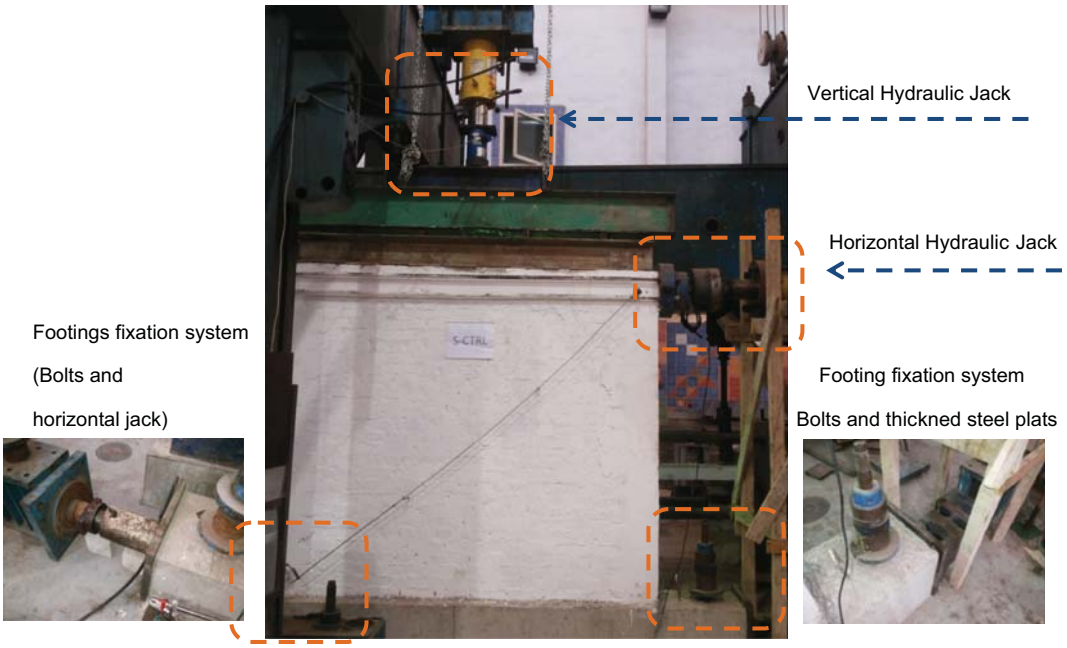

Fig. 7. Test setup, boundary conditions and loading mechanism.

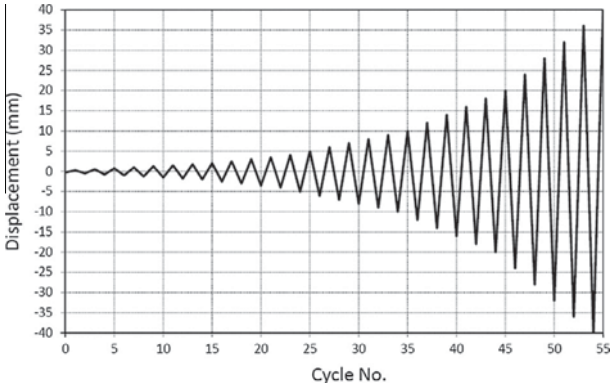

Fig. 8. Cyclic displacement protocol.

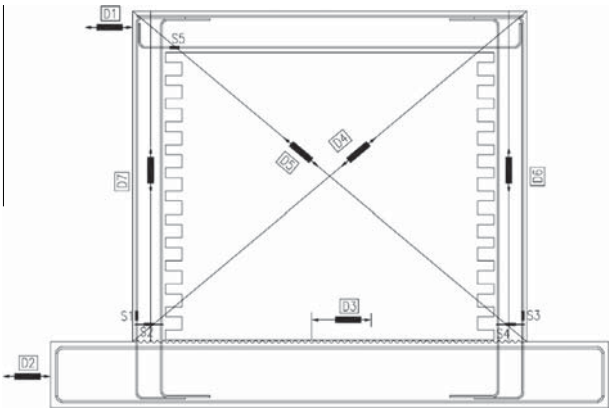

Fig. 9. Instrumentation scheme.

suggested. And the accuracy of the prediction method could be verified, and the applicability of its model in analysis was confirmed using pushover analysis.

A mathematical model was developed by Flores and Alcocer [11] to represent the non-linear behavior of confined masonry structures built with hand-made clay bricks. The suggested envelope curve of the model is a tri-linear force–deformation curve, which is calculated from material properties and wall geometry. The parameters for envelope curve are detailed according to masonry walls with and without horizontal reinforcement at

Fig. 10. Crack pattern for CLY-S-CTRL.

Fig. 11. Crack pattern for CLY-S-FERRO-C.

bed joints. Also an experimental study on effects of height of lateral forces, column reinforcement and wall reinforcements on seismic behavior of confined masonry was developed by Yoshimura et al. [12] to study the ultimate shear strengths of the confined concrete hollow block masonry specimens with developed equation.

ElGawady et al. [13] conducted dynamic in-plane tests on six slender un-reinforced masonry walls retrofitted using different types of FRP and were subjected to a series of simulated earthquake motions on an earthquake simulator. It was observed that FRP upgrading improve the wall lateral resistance by a factor ranging from 1.3 to 2.9 and the X shape upgrading configuration had the maximum drift of all specimens.

Grids of GFRP were used by Yu et al. [14] to reinforce a fast setting polyurea spray to strengthen eleven URM walls subjected to in-plane diagonal compressive load and it was concluded that the failure mode was directly affected by strengthening schemes (orientations) and the lateral load capacity increased by a factor of 1.1–1.43 for brick walls and 1.1–1.6 for concrete block walls.

As a part of a research program aiming at developing structurally and economically efficient hybrid building system for developing countries in general and for Egypt in particular. This paper investigates the lateral load behavior of retrofitted confined masonry walls using low cost ferrocement and GFRP systems designed and built using locally available materials and with common workmanship and construction practice.

2. Experimental program

The experimental program investigates the effectiveness of composite materials; namely ferrocement using expanded mesh and sheets of glass woven textile fibers (GFRP), as externally bonded upgrading materials for the in-plane retrofitting of CM walls. The two alternatives represent low-cost retrofitting methods. The experimental program includes testing both

Fig. 12. Crack pattern for CLY-S-FERRO-X with rocking at connection.

Fig. 13. Crack pattern for CLY-S-GFRP-X with rocking at connection.

Fig. 14. Crack pattern for CLY-S-FERRO-F with enlarged rocking at connection.

Fig. 15. Crack pattern for CLY-S-GFRP-F with enlarged rocking at connection.

Fig. 16. Crack pattern for CLY-P-W.

Fig. 17. Crack pattern for CLY-W-FERRO.

un-retrofitted and retrofitted CM wall assemblies up to failure under reversed cyclic lateral loads.

2.1. Description of the tested walls

Ten wall assemblies with a 0.80-scale were built, using 0.80-scale clay brick units. The assemblies consisted of a clay masonry panel, two confining columns and a tie beam. The assemblies were tested under a combination of a constant vertical load and lateral cyclic loading with displacement controlled loading protocol up to failure. Table 1 summarizes the tested walls. The walls were selected such that it covers the range of different perforations, namely solid walls or walls with window or door openings. The test matrix investigates the use of ferrocement or GFRP in retrofitting these alternatives using multiple arrangements. Coverage of the walls was done either by fully covering the entire wall with the confining elements, covering the corners of the panel with an overlap with the confining elements or by forming a diagonal X-brace in the masonry panel. Typical details of tested walls are shown in Fig. 1. The construction of wall assemblies is shown in Fig. 2a–d, the thickness of wall for all assemblies was 200 mm.

Five walls were retrofitted using one ferrocement layer consisting of expanded wire mesh with a grid size of 15 × 35 mm and thickness of 1.6 mm, the mesh was from mild steel (Grade 240/350) with yield stress (f_y) of 240 MPa, and ultimate tensile strength (f_u) of 350 MPa and modulus of elasticity (E_s) of 200 GPa. The expanded mesh was fixed to the masonry wall after spatter-dashing it by nails every 100 mm in both directions, then covering the expanded mesh with a mortar of 20 mm thickness as shown in

Fig. 18. Crack pattern for CLY-P-D.

Fig. 19. Crack pattern for CLY-D-FERRO.

Fig. 3. The mortar characteristics (3 sand: 1 cement & w/c ratio of 0.5). The 28-days characteristic compressive strength of mortar, (f_{cu}), was on average 21.8 MPa.

The assemblies CLY-S-FERRO-C and CLY-S-FERRO-X were covered by two perpendicular expanded meshes for each face with mortar thickness of 30 mm.

Two walls were retrofitted using GFRP sheets. Firstly a thin layer of mortar was applied on the masonry panel to make the surface of as plane as possible, then the surface was painted by a layer of polyester resin and the GFRP sheets with properties as mentioned in Table 2. Fig. 4 shows the retrofitting procedures.

For control purposes, standard concrete cubes were cast alongside the walls and were tested at the same day as the walls, the 28-days concrete characteristic compressive strength, (f_{cu}), was on average 25.4 MPa. Standard five brick masonry prisms were built next to the walls and tested at the same day of the wall testing. The mean compressive strength of the clay masonry prisms (f'_m) was 5.7 MPa. The longitudinal reinforcement of beams and columns was made of deformed steel bars (Grade 360/520) of yield stress (f_y) of 360 MPa, and ultimate tensile strength (f_u) of 520 MPa. The transverse reinforcement was made of mild steel smooth bars (Grade 240/350) of yield stress (f_y) of 240 MPa, and ultimate tensile strength (f_u) of 350 MPa. All the previous reinforcement had a modulus of elasticity (E_s) of 200 GPa. The walls were left to cure for 28 days before testing and were white washed with non-latex paint to ease the visualization of the developed cracks during tests.

Two masonry wallets with size (850 × 850 × 95 mm) were built next to the walls. The wallets tested by diagonal compression test as per ASTM E519-02 [15] to determine the diagonal tensile strength; a schematic test setup of diagonal compression test is shown in Fig. 5.

The test setup is composed of two steel loading shoes, which were fixed on the two opposite corners on the wallet. The load is applied to the wallet by a hydraulic jack on the steel loading shoes positioned on top of the specimen and transmitted to the other shoe which was placed at the bottom of the specimen.

The test was introduced to simulate a pure shear stress state, the ASTM [15] assumes that the diagonal compression test produces a uniform shear stress and a Mohr's circle centered in the origin of the Cartesian system of axis. In that case the value of the shear stress τ is equal to the principal tensile stress f_t. The shear stress τ is obtained by Eq. (1):

$$\tau = \frac{0.707\,P}{A_n} \tag{1}$$

where P is the load applied by the jack and A_n is the net area of the specimen, calculated as follows:

$$A_n = \left(\frac{w+h}{2}\right) \cdot t \cdot n \tag{2}$$

where w is the specimen width, h is the specimen height, t is the thickness of the specimen and n is the percentage of the unit's gross area that is solid, expressed as a decimal. In the present work the value $n = 0.84$ was adopted. The same expressions are also presented in Eurocode 6 [16].

The RILEM committee [17] considers that the stress field is not uniform and proposes the following expression to evaluate the tensile strength of masonry:

$$f_t = \frac{0.5\,P}{A_n} \tag{3}$$

Fig. 6a and b shows the failure and crack patterns for both wallets W1 and W2, both of them shared the same mode of failure characterized by direct diagonal tension crack under failure loads of 105 and 111 kN respectively.

According to Eq. (3), the tensile stress f_t for specimens equals 0.77 and 0.81 MPa respectively.

2.2. Test setup, boundary conditions and loading scheme

The walls were tested up to failure under a combined constant vertical load and in-plane cyclic lateral load, Fig. 7 shows the test setup of the walls. In this respect, a single concentrated load of 250 kN (for all walls except 500 kN for specimen CLY-S-GFRP-F) was firstly distributed by a stiff steel distributor I-beam laid on top of secondary steel beam and separated by four rolling steel cylinders as shown in Fig. 7. The secondary steel beam was laid on top of the concrete tie beam of the assembly using gypsum bedding to avoid stress concentration. The purpose of the rolling cylinders is to allow the wall to displace laterally while maintaining the distributed vertical load. The load was chosen to simulate that of a typical module in a five-story residential building with commonly used module dimensions. The lateral cyclic load was applied using a 900 kN hydraulic actuator. The horizontal action is applied to the wall via control displacement at a rate of 60 μm/s, full displacement protocol was programmed for each amplitude increment aiming at strength and degradation assessment as shown in Fig. 8. The footing was fixed to the reaction floor by two strong pre-tensile bolts (Ø50 mm) spaced by 3.0 m to prevent overturning and sliding of the footing during test, in addition, a horizontal hydraulic jack was placed horizontally at footing level and reacting against a steel reaction column, in the opposite

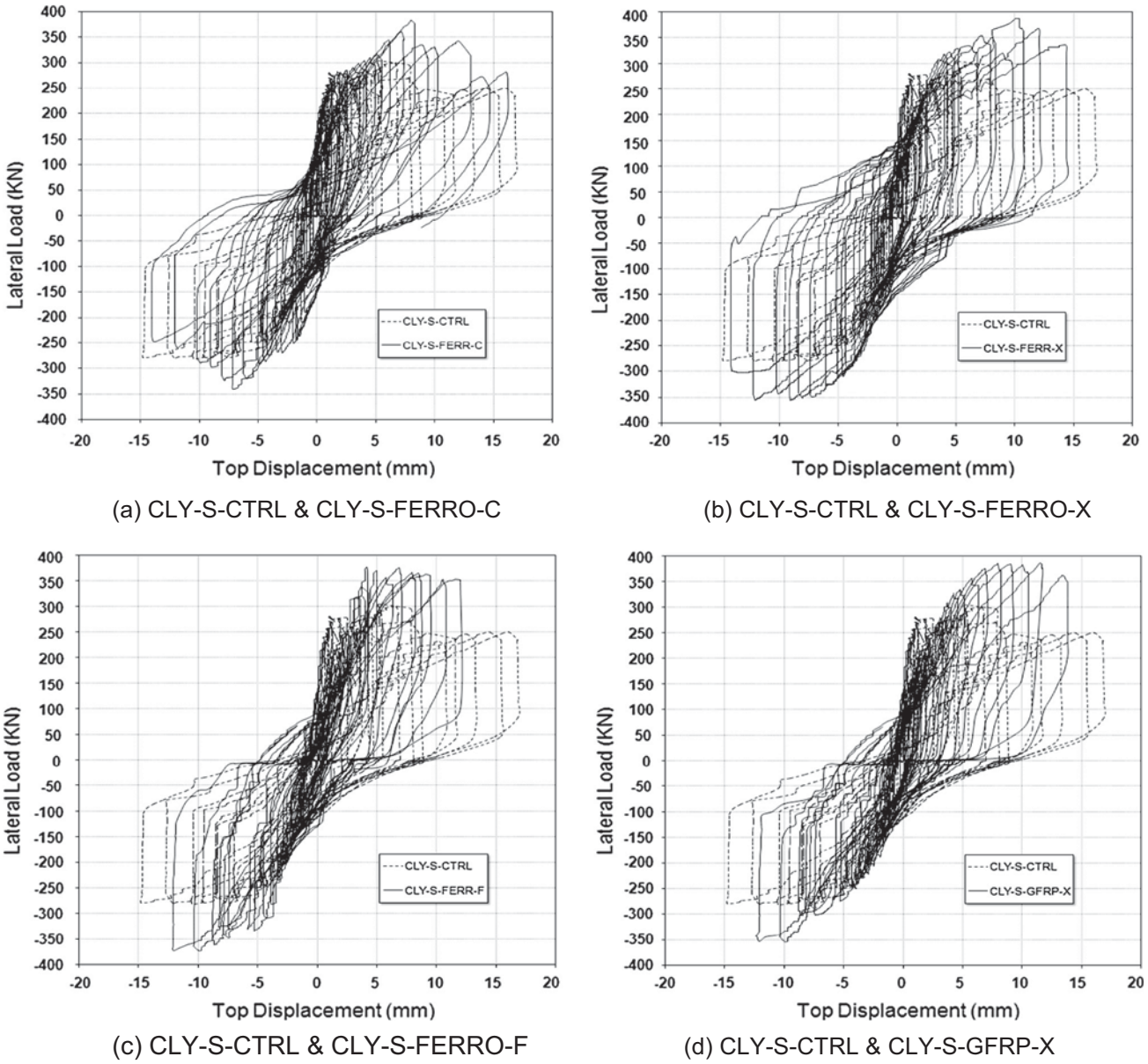

Fig. 20. Hysteretic curves for retrofitted and un-retrofitted solid walls.

side a thick steel plates were placed to restrain the sliding of footing during the test as shown in Fig. 7. At the end of each cycle, the displacement was held constant for a period of 2 min, during which measurements, observations as well as marking of the visible cracks too place.

2.3. Instrumentation

Measurements were made for displacements, steel, and concrete strains at key locations of the tested walls, displacement were measured using six 0.01 mm accuracy electrical linear variable distance transducers (LVDTs), coded (D), positioned as shown on Fig. 9. The steel strain in the longitudinal and transverse reinforcement was monitored using five electrical strain gauges of 10 mm gauge length and 120 Ohm resistance, coded (S), as shown in Fig. 9. All LDVTs and strain gauges were connected to a computer controlled data acquisition system. The crack patterns was continuously monitored and printed on the walls with the associated displacement level printed next to it.

3. Experimental observations and discussion

3.1. Failure pattern

Fig. 10 shows the failure and crack pattern for the un-retrofitted wall (CLY-S-CTRL) the mode of failure may be characterized by shear failure of the confining columns and diagonal bed-joint cracking of the masonry panel. It is worth nothing that no separation was observed at the toothed interface between the confining columns and the masonry panel, clearly confirming a significant difference between infilled frames and confined masonry panel.

Fig. 11 shows the failure and crack pattern for the retrofitted solid wall (CLY-S-FERRO-C), it can be clearly seen that the presence of the ferrocement layers at corners delay the diagonal shear cracks in masonry panel to propagate in confining column which occurred in the un-retrofitted wall, later the failure was due to diagonal shear cracks developing around the retrofitted corners. The failure occurred at increased capacity and ductility.

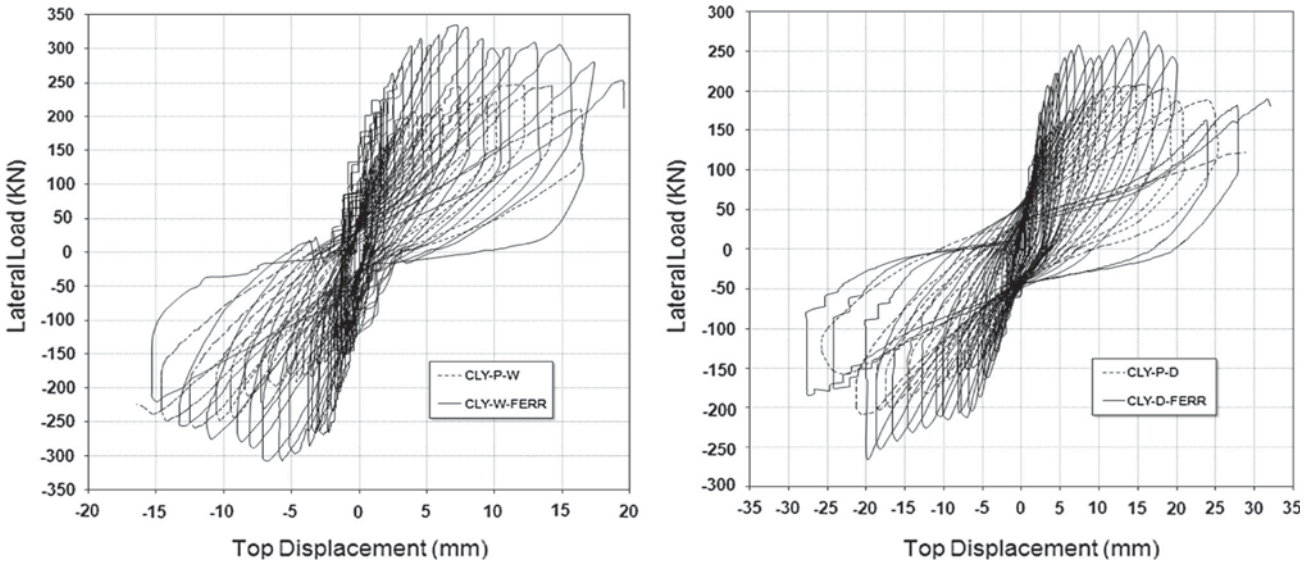

Fig. 21. Hysteretic curves for retrofitted and un-retrofitted perforated walls.

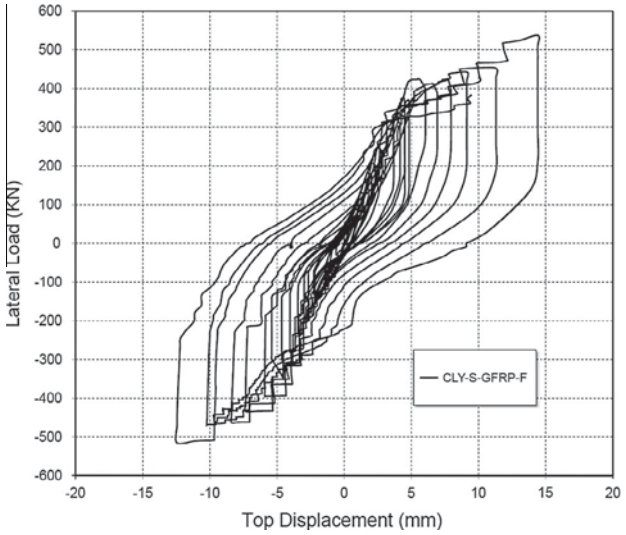

Fig. 22. Hysteretic curve for wall CLY-S-GFRP-F.

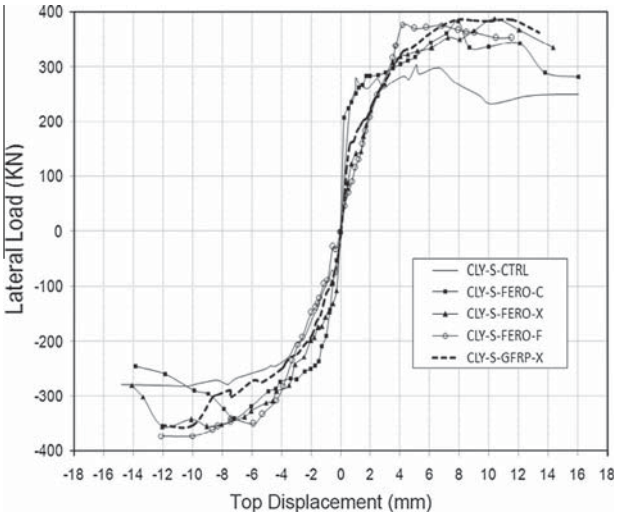

Fig. 23. Envelope curves for solid walls.

Fig. 12 shows the failure and crack pattern for the retrofitted solid wall (CLY-S-FERRO-X), it can be clearly seen that the presence of the ferrocement layers on the path of the principle tension fields prevented the diagonal shear cracks in masonry panel, later some minor flexural cracks were seen in the confining columns, the failure was due to rocking for the undamaged panel after the slightly reinforced confining column reached its ultimate tension capacity at base. The failure mode of the retrofitted wall (CLY-S-GFRP-X) was similar to specimen (CLY-S-FERRO-X) as shown in Fig. 13.

For the retrofitted solid wall (CLY-S-FERRO-F), the presence of a full coverage with ferrocement layers prevented any cracks in masonry panel and the confining elements. The failure was due to rocking for the un-cracked panel as shown in Fig. 14. The failure mode of the retrofitted wall (CLY-S-GFRP-F) was similar to specimen (CLY-S-FERRO-F) as shown in Fig. 15.

Figs. 16 and 17 clarify the difference of failure mode for both un-retrofitted and retrofitted walls with window opening. The presences of ferrocement layer prevent shear failure of confining

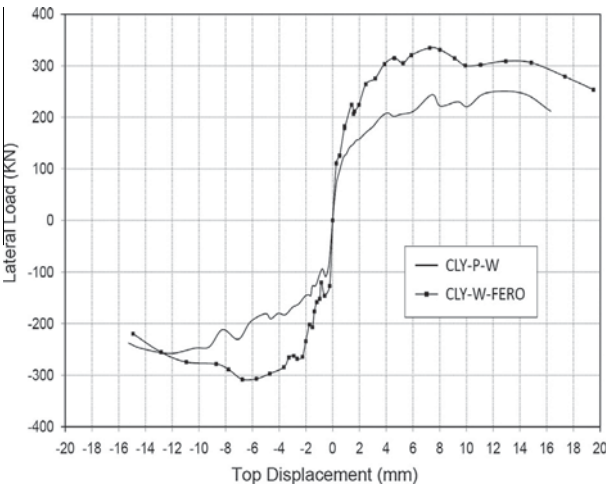

Fig. 24. Envelope curves for walls with window.

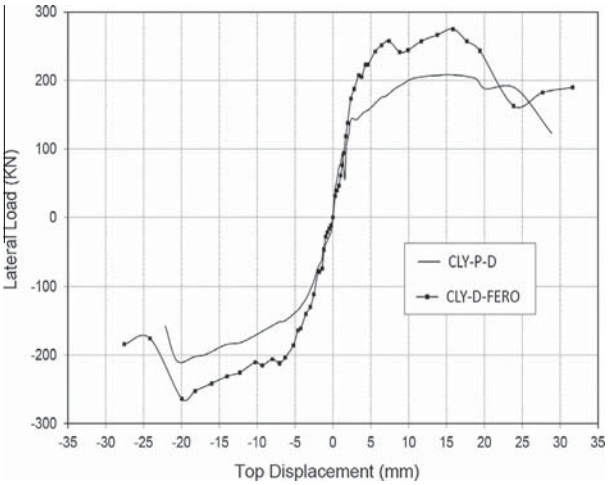

Fig. 25. Envelope curves for walls with door.

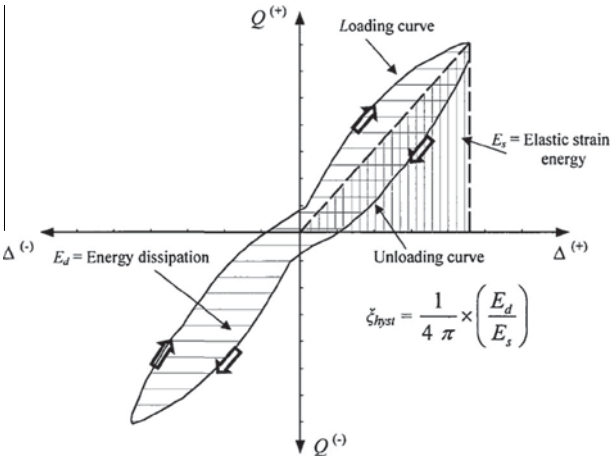

Fig. 26. Calculation of energy dissipation.

columns and minimized the cracks in the masonry panel. The failure occurred at increased capacity and ductility as will be described in details in a later section. It can be clearly noticed that the shear failure in the confining elements was shifted to diagonal cracks in the masonry panel around the window opening.

The failure pattern of the un-retrofitted wall with door opening may be characterized by shear failure with diagonal struts forming in the two piers, as shown in Fig. 18, the presence of ferrocement layer prevented these diagonal shear cracks in piers, later at higher levels of lateral loads the failure was due to the rocking of the piers and the door lintel due to the formation of plastic hinges at their ends, as shown in Fig. 19.

3.2. Behavior of retrofitted walls

Wall assembly CLY-S-FERRO-C was retrofitted using two layers of ferrocement at connections on both sides. The wall's ultimate load was 383 kN as opposed to 304 kN for the reference un-retrofitted wall (CLY-S-CTRL). This corresponding to about 26% increase in the lateral load resistance of the wall. Fig. 20a shows the hysteretic curves for both assemblies.

Wall assembly CLY-S-FERRO-X was retrofitted using two layers of ferrocement at diagonals on both sides. The wall's ultimate load was 387 kN as opposed to 304 kN for the reference un-retrofitted wall (CLY-S-CTRL). This corresponding to about 27.5% increase in the lateral load resistance of the wall. Fig. 20b shows the hysteretic curves for both assemblies.

Wall assembly CLY-S-FERRO-F was retrofitted using one layer of ferrocement covering full masonry panel on both sides. The wall's ultimate load was 377 kN as opposed to 304 kN for the reference un-retrofitted wall (CLY-S-CTRL). This corresponding to about 24% increase in the lateral load resistance of the wall. Fig. 20c shows the hysteretic curves for both assemblies.

Wall assembly CLY-S-GFRP-X was retrofitted two layers of GFRP sheets at diagonals on both sides. The wall's ultimate load was

Table 3
Summary of test results.

Wall ID	Direction	Maximum load		Displacement relative to maximum load		Cracking load		Maximum displacement	
		Load (kN)	Variation%	Drift (mm)	Variation%	Load (kN)	Variation%	Drift (mm)	Variation%
CLY-S-CTRL	Push	300	–	7	–	250	–	16	–
	Pull	−280	–	−10	–	−170	–	−14.8	–
CLY-S-FERRO-C	Push	380	27[a]	8	14[a]	340	36[a]	16.2	1[a]
	Pull	−350	25[a]	−7	−30[a]	−350	106[a]	−14	−5[a]
CLY-S-FERRO-X	Push	387	29[a]	10.5	50[a]	330	32[a]	14.1	−11[a]
	Pull	−370	32[a]	−12	20[a]	−340	100[a]	−14	5[a]
CLY-S-GFRP-X	Push	386	29[a]	11	57[a]	330	32[a]	13.8	−14[a]
	Pull	−360	29[a]	−10.5	5[a]	−300	76[a]	−12.2	−17[a]
CLY-S-FERRO-F	Push	377	26[a]	7	0.5[a]	377	51[a]	11.8	−26[a]
	Pull	−375	34[a]	−10	0.4[a]	−375	121[a]	−12.1	−18[a]
CLY-S-GFRP-F	Push	540	n/a	14	n/a	540	n/a	14	n/a
	Pull	−510	n/a	−13	n/a	−510	n/a	−13	n/a
CLY-P-W	Push	250	–	12	–	155	–	16.2	–
	Pull	−258	–	−10	–	−150	–	−15	–
CLY-W-FERRO	Push	335	34[b]	7.3	−39[b]	225	45[b]	19.2	19[b]
	Pull	−315	22[b]	−7	−30[b]	−230	53[b]	−15	0.3[b]
CLT-P-D	Push	205	–	15	–	140	–	27	–
	Pull	−209	–	−20	–	−120	–	−22.5	–
CLY-D-FERRO	Push	270	32 [c]	16	7[c]	210	50[c]	34	26 [c]
	Pull	−275	32 [c]	−20	0.4[c]	−145	21[c]	−27.5	22 [c]

[a] Percentage referenced to the specimen (CLY-S-CTRL).
[b] Percentage referenced to the specimen (CLY-P-W).
[c] Percentage referenced to the specimen (CLY-S-CTRL).

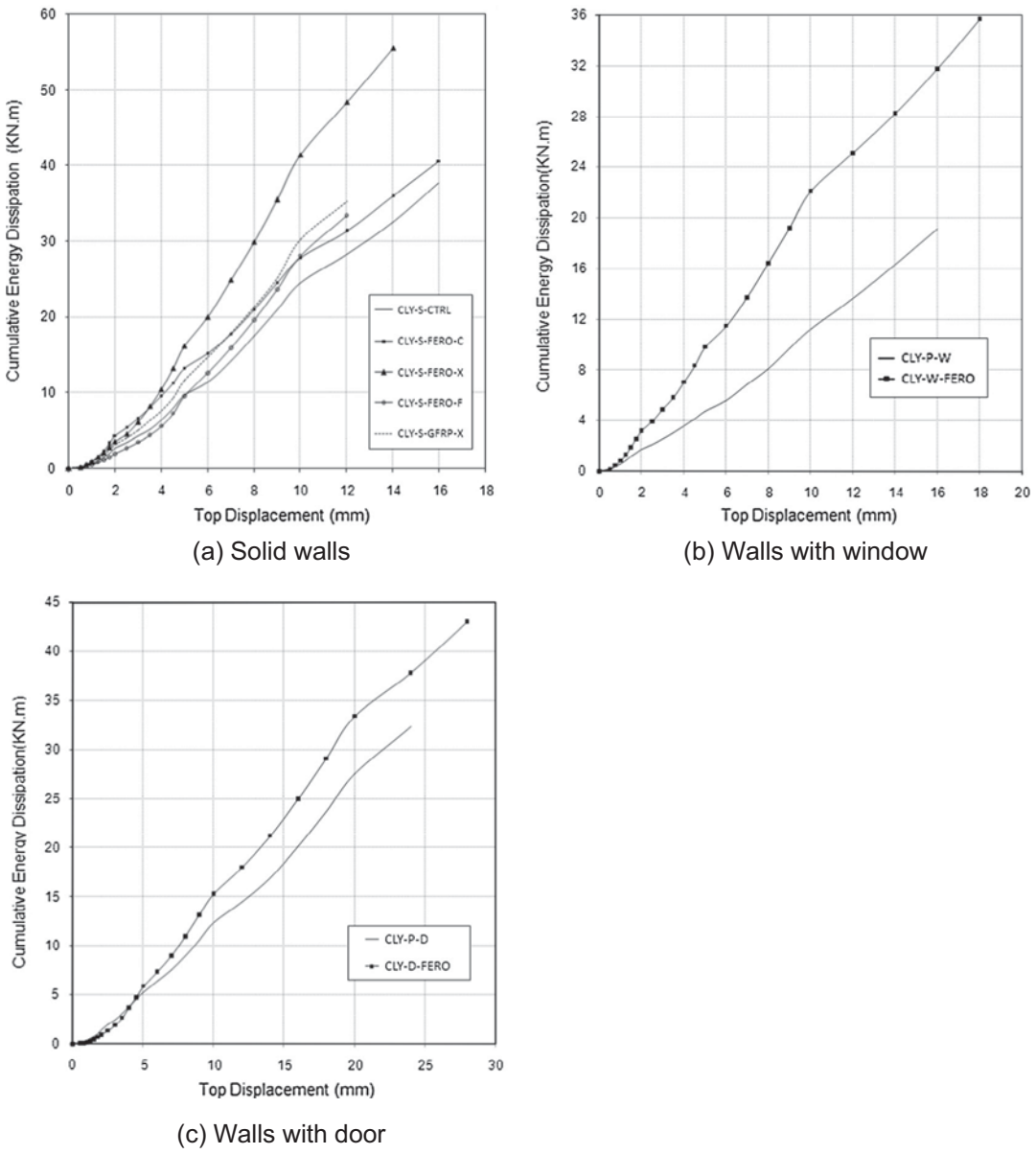

Fig. 27. Cumulative energy dissipation for wall assemblies.

386 kN as opposed to 304 kN for the reference un-retrofitted wall (CLY-S-CTRL). This corresponding to about 27% increase in the lateral load resistance of the wall. Fig. 20d shows the hysteretic curves for both assemblies.

Wall assembly CLY-W-FERRO was retrofitted using one layer of ferrocement covering full masonry panel on both sides. The wall's ultimate load was 335 kN as opposed to 258 kN for the reference un-retrofitted wall (CLY-P-W). This corresponding to about 30% increase in the lateral load resistance of the wall. Fig. 21a shows the hysteretic curves for both assemblies.

Wall assembly CLY-D-FERRO was retrofitted using one layer of ferrocement covering full masonry panel on both sides. The wall's ultimate load was 275 kN as opposed to 209 kN for the reference un-retrofitted wall (CLY-P-D). This corresponding to about 32% increase in the lateral load resistance of the wall. Fig. 21b shows the hysteretic curves for both assemblies. Envelope curves for solid and perforated walls are shown in Figs. 23–25.

Wall assembly CLY-S-GFRP-F was retrofitted using one layer of GFRP sheets covering full masonry panel on both sides and tested under constant vertical stress of 1.0 MPa. The wall's ultimate load was 540 kN. Fig. 22 shows the Hysteretic curve for the wall assembly. Table 3 summarizes all test results for both un-retrofitted and retrofitted walls.

3.3. Energy dissipation

Energy dissipation, E_d, through hysteresis damping is an important aspect in seismic design response, E_d, has been represented, as suggested by Hose and Seible [18], by area enclosed within the force–displacement curve at each displacement level. This is the horizontally-hatched area shown in Fig. 26. The vertically-hatched region in the same figure represents the elastic strain energy, E_s, stored in an equivalent linear elastic system.

The cumulative energy dissipation at different displacement levels of solid wall assemblies were presented in Fig. 27a. The figure showed that, an improvement in total energy dissipation of about 47% has been achieved for the retrofitted assembly CLY-S-FERRO-X corresponding to the control solid assembly CLY-S-CTRL.

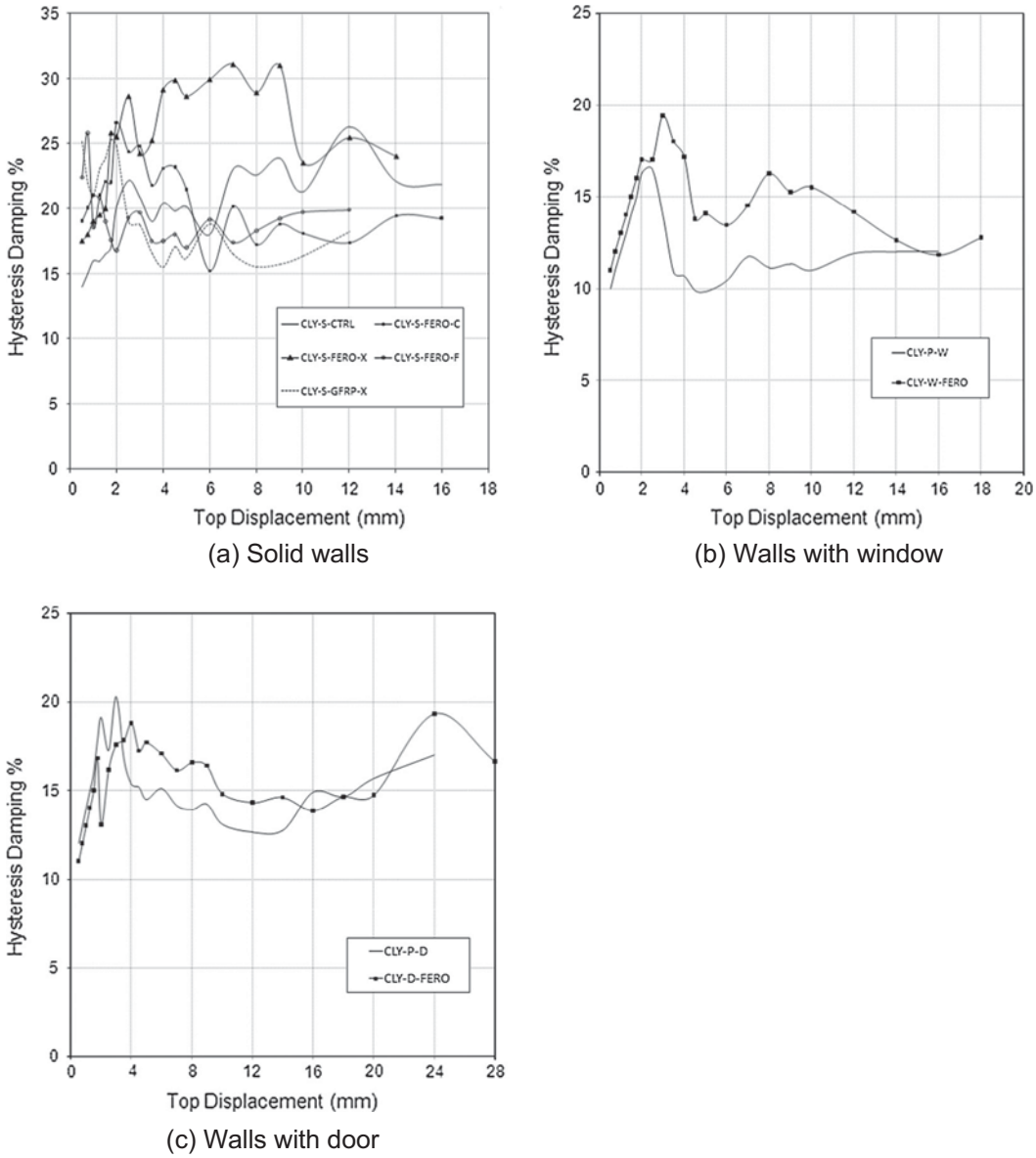

Fig. 28. Hysteresis damping percentages for wall assemblies.

Fig. 27b shows the cumulative energy dissipation for assemblies CLY-P-W AND CLAY-W-FERRO, an improvement in total energy dissipation of about 85% was achieved.

An improvement of total energy dissipation of about 33% was achieved for wall assembly CLY-P-D as shown in Fig. 27c.

3.4. Hysteretic damping

Hysteretic damping, ξ_{hyst}, can be quantified based on the equal area approach (Hose and seible [18]) that represents the same amount of energy loss per loading cycle. The relationship between the dissipated energy, E_d, the stored strain energy, E_s, and the hysteretic damping is given by equation shown in Fig. 26.

The hysteretic damping was plotted against lateral top displacement for solid and perforated walls are shown in Fig. 28a–c.

For the solid walls, the hysteretic damping ranges from 15% to 30% and the wall assembly CLY-S-FERRO-X was the largest percentage ranging from 22.5% to 32%.

An improvement in hysteretic damping was achieved for the retrofitted perforated walls with windows and doors as shown in Fig. 28b and c.

3.5. Stiffness degradation

To assess the variation in wall stiffness with increased loading and top displacement, the secant stiffness, defined as the ratio between the lateral resistance and the corresponding top lateral wall displacement, was used. The cycle stiffness of the specimen at a certain displacement level was considered as the average of stiffness in the positive and negative loading directions, as illustrated in Fig. 29a–c.

The trends of stiffness degradation for all walls were approximately similar and showed significant decreases with increased top displacement.

4. Numerical analysis

The aim of this section is to establish a simple three-dimensional nonlinear model for the tested wall assemblies that are capable of capturing the key response features of the failure mode shapes and crack patterns for each assembly and comparing it with experimental results and with respect to the past references.

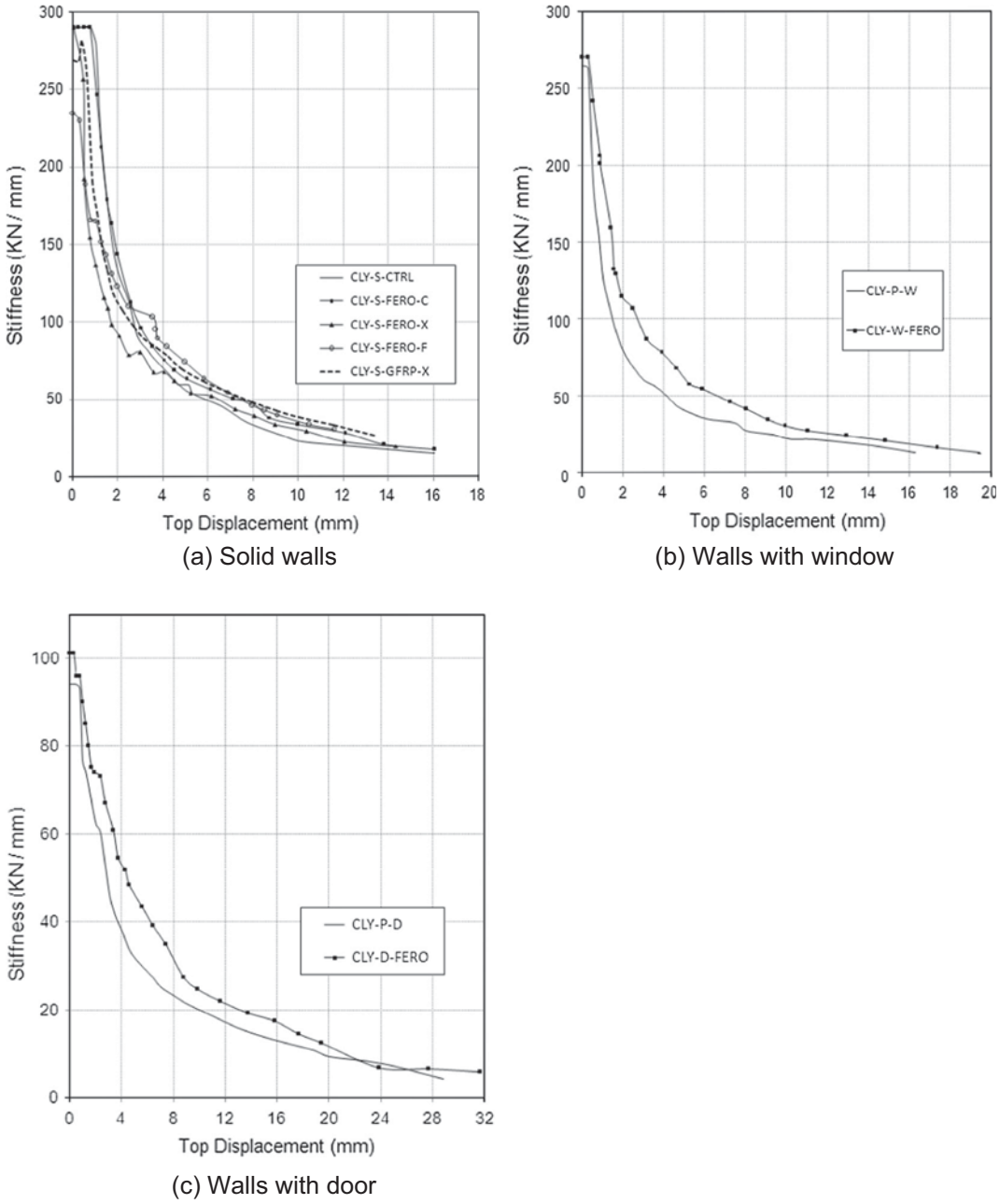

Fig. 29. Stiffness degradation for wall assemblies.

In the past, numerous studies were conducted on the finite element models of masonry walls as well as RC infilled frames. Kaushik et al. [19] studied the uniaxial monotonic compressive stress–strain behavior and estimated the modulus of elasticity of bricks, mortar, and masonry as 300, 200, and 550 times their compressive strengths, respectively.

There are two methods of finite element modeling for masonry structures which consist of bricks and mortar: separated modeling and integrated modeling. The former simulates brick and mortar separately while the later simulates them integrity. For the separated modeling approach, there are two categories: the first assumes that brick and mortar are well integrated, and the element nodes on the contact surface satisfy continuous displacement condition. Hence, the degrees of freedom on the corresponding nodes on the contact surface are coupled together. The other one considers bond-slip between brick and mortar, which requires the introduction of interface elements (Huang et al. [20]).

Analysis on the characteristics and features of masonry using Solid65 elements in "ANSYS® [21]" was studied by Huang et al. [20] with the shear property of joints in masonry structures under different vertical load (σ/fm) was numerically simulated. Comparing the experimental results with the numerical ones, the proposed values for the shear transfer coefficients for open and closed crack of Solid65 elements for simulating masonry structures were suggested.

4.1. Finite element model

The non-linear finite elements analysis was carried out using a computer package "ANSYS® [21]". An 8-node solid element with three translational and additional rotational degrees of freedom at each node was chosen to idealize the concrete and masonry (SOLID65) whereas a 2-node bar element was used to model the steel rebars (LINK8). Typical modeling of the column and beam

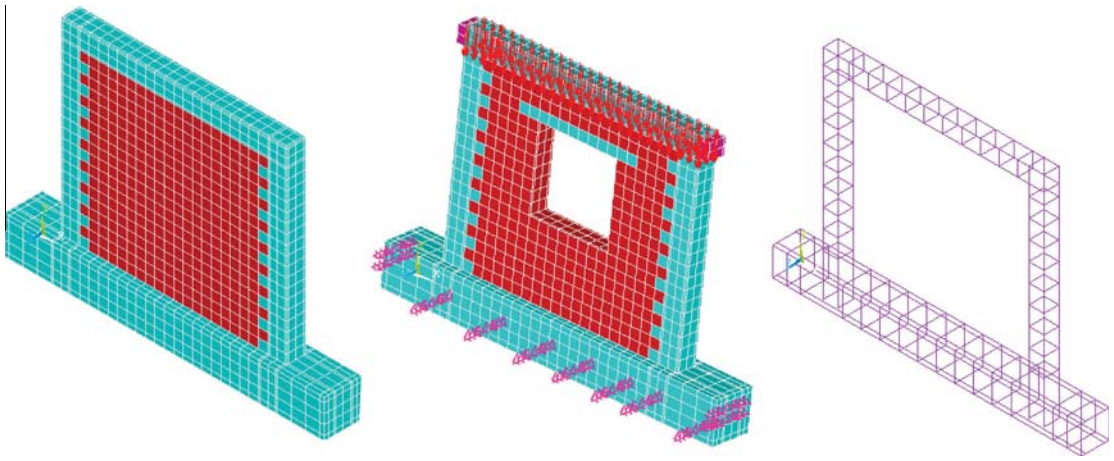

Fig. 30. Finite element model characterization and meshing.

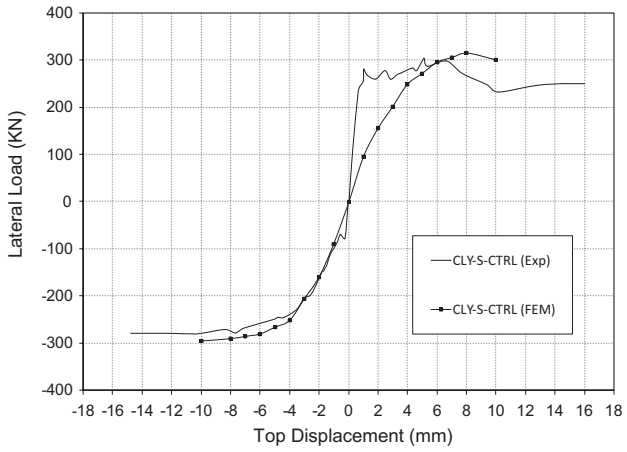

Fig. 31a. Envelope load–displacement curves for wall assembly CLY-S-CTRL.

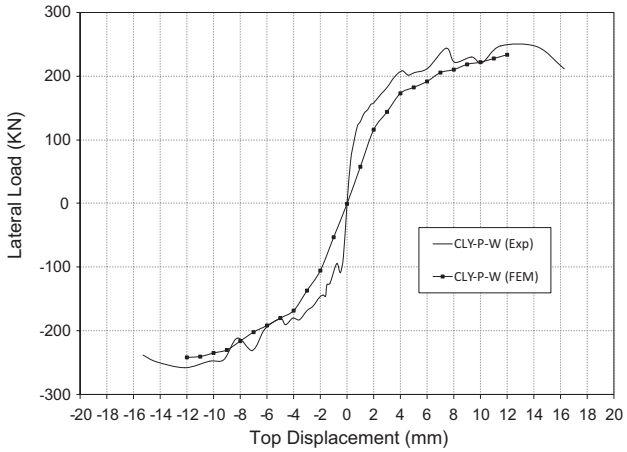

Fig. 31b. Envelope load–displacement curves for wall assembly CLY-P-W.

elements representing the concrete and steel rebars is indicated in Fig. 30 with the boundary conditions. The loading of the model was similar to that conducted in the experimental program, where a total vertical load of 250 kN was applied uniformly on the top beam then an incremental displacement cyclic load was applied

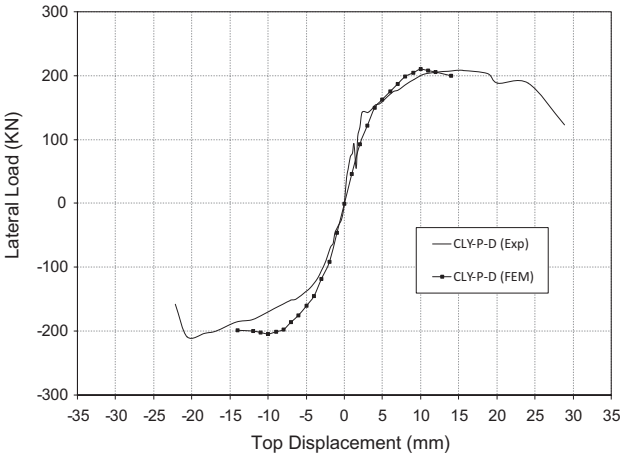

Fig. 31c. Envelope load–displacement curves for wall assembly CLY-P-D.

at the top of the confined column according to same displacement protocol of experimental tests until failure occurs. As stated before from experimental results no separation was observed at the toothed interface between the confining columns and the masonry panel for all wall assemblies under large deformation so the interface between the masonry panel and the concrete frame was modeled as full bond with the corresponding mechanical properties for each material with respect to the stress strain curves for masonry suggested by Kaushik et al. [19].

The concrete material model in ANSYS uses a failure model developed by Willam and Warnke [22] for multiaxial stress state. Solid65 element decides the cracking and crushing of concrete through this material model. A material model may be composed of two or more material definitions. Concrete and masonry materials should have at least Elastic and Concrete material definitions. In Elastic definition, the modulus of elasticity and Poisson's ratio are necessary. For Concrete definition, axial tension strength for concrete and masonry and shear transfer coefficients between crack surfaces for open and closed cracks are required. If the shear transfer from one crack surface to the other does not exist then the shear transfer coefficient is 0.0, if it fully exists then the coefficient is 1.0. In the literature, there are different suggestions for this coefficient by researchers, the suggest values here were 0.3 and 0.6 for open and closed cracks respectively for masonry as suggested by Sandeep et al. [23].

Table 4
Summary of finite element model vs. test results.

Wall ID	Direction	Maximum load (kN)			Displacement relative to maximum load (mm)			Cracking load (kN)			Maximum displacement (mm)		
		Exp.	F.E.M	$\frac{\text{Exp.}}{\text{F.E.M.}}$	Exp.	F.E.M	$\frac{\text{Exp.}}{\text{F.E.M.}}$	Exp.	F.E.M	$\frac{\text{Exp.}}{\text{F.E.M.}}$	Exp.	F.E.M	$\frac{\text{Exp.}}{\text{F.E.M.}}$
CLY-S-CTRL	Push	300	315	0.95	7	8	0.88	250	150	1.67	16	10	1.60
	Pull	−280	−295	0.95	−10	−10	1.00	−170	−155	1.10	−14.8	−10	1.48
CLY-P-W	Push	250	233	1.07	12	12	1.00	155	140	1.11	16.2	12	1.35
	Pull	−258	−242	1.07	−10	−12	0.83	−150	−136	1.10	−15	−12	1.25
CLY-P-D	Push	205	210	0.98	15	10	1.50	140	120	1.17	27	14	1.93
	Pull	−209	−204	1.02	−20	−10	2.00	−120	−110	1.09	−22.5	−14	1.61

Fig. 32a. Crack pattern for CLY-S-CTRL.

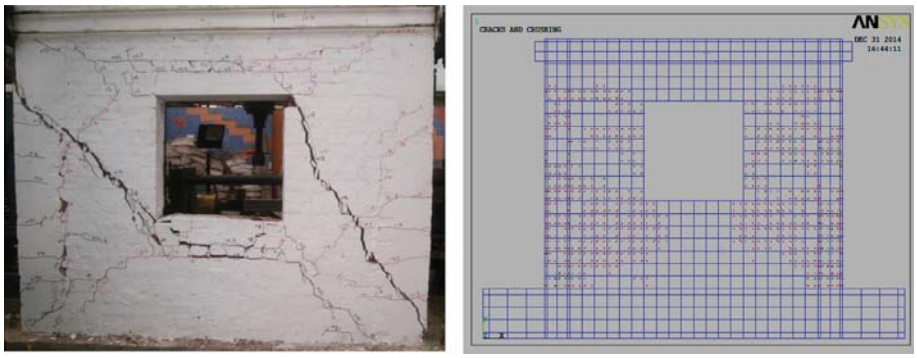

Fig. 32b. Crack pattern for CLY-P-W.

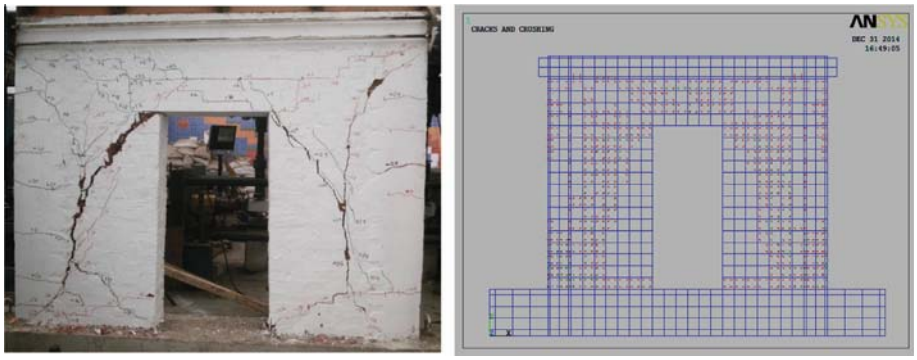

Fig. 32c. Crack pattern for CLY-P-D.

4.2. Implementation and numerical evaluation

The correlation between experimental and numerical results is based on comparisons of failure modes, cracking patterns and plastic hinge locations as well as load–displacement curves.

The predicted lateral load capacity and failure mode obtained from the model was examined against the test results for each wall specimens. Figs. 31a–31c show the load–displacement envelope curves from the test and the finite element model for the solid wall panels (CLY-S-CTRL), wall panel with window opening (CLY-P-W), and wall panel with door opening (CLY-P-D) respectively. Comparisons of maximum and ultimate loads with their corresponding displacements for models and experimental results are summarized as shown in Table 4.

The cracking patterns for the finite element models for each wall assembly as compared to the experimental test results are shown in Figs. 32a–32c.

Results from the finite element analysis of showed that the developed models are capable with sufficient degree of accuracy to capture the maximum load and its corresponding deformation of the tested walls except for corresponding deformation for wall CLY-P-D. The ultimate displacements in models were less than its in experimental works which indicated that the plastic analysis needs to be enhanced.

The proposed model showed good agreement with the results of the laboratory tests for crack patterns and failure mechanisms for all models as shown in Figs. 32a–32c.

5. Summary and conclusions

This paper presents results of cyclic loading tests investigating the in-plan behavior of confined masonry walls retrofitted using low cost ferrocement and GFRP. Ten walls with scale of 0.8 were built, using 0.8 scale brick clay units, consisting of a clay masonry panel, two confining columns and a tie beam, were tested under a combination of a constant vertical load and lateral cyclic loading with displacement control protocol up to failure. Wall panels had various configurations, namely, six solid walls, two perforated walls with window openings and two with door openings. Two composite materials (ferrocement and GFRP) and three retrofitting configurations (diagonal "X", connection, and full coverage) were investigated. Key research findings may be summarized as follows:

1. The upgrading techniques improved the lateral resistance of the confined walls by a factor ranging from 25% to 32% and also improve the total energy dissipation by a factor ranging from 33% to 85%.
2. The upgrading configurations of diagonal "X" and full coverage can help prevent diagonal shear failure especially in tie columns and convert failure mode to rocking mode for the undamaged masonry panel. Additionally, in all situations, it will postpone collapse by "keeping the bricks together" under large seismic deformations.
3. The improvement in maximum lateral drifts was less significant.
4. Ferrocement and the low cost GFRP sheets showed a similar enhancement for solid panels without any de-bonding under high levels of lateral loading.
5. The proposed finite element models showed good agreement with the results of the laboratory tests for crack patterns and failure mechanisms for all models and for maximum load ant its corresponding deformation for most cases.
6. The proposed finite element models showed good agreement with the results of the laboratory tests for maximum load and its corresponding deformation for most cases.

References

[1] Brzev S. Earthquake-resistant confined masonry construction. India: National Information Center of Earthquake Engineering, Indian Institute of Technology Kanpur; 2008.
[2] Yoshimura K, Kikuchi K, Kuroki M, Nonaka H, Tae Kim K, Wangdi R, Osikata A. Experimental study for developing higher seismic performance of brick masonry walls. In: 13th World conference on earthquake engineering, Vancouver, B.C., Canada, No. 1597; 2004.
[3] Riahi Zahra, Elwood Kenneth J, Alcocer Sergio M. Backbone model for confined masonry walls for performance-based seismic design. J Struct Eng 2009;135(6):644–54.
[4] Tomazevic M, Klemence I. Verification of seismic resistance of confined masonry buildings. Earthquake Eng Struct Dyn 1997;26:1073–88.
[5] Tomazevic M. Earthquake-resistant design of masonry buildings. London, U.K: Imperial College Press; 1999.
[6] Tu YH, Chuang TH, Liu PM, Yang YS. Out-of-plane shaking table tests on unreinforced masonry panels in RC frames. Eng Struct 2010;32:3295–935.
[7] Ishibashi K, Meli R, Alcocer SM, Leon F, Sanchez TA. Experimental study on earthquake-resistant design of confined masonry structure. In: Proceedings of the tenth world conference on earthquake engineering, Madrid, Spain; 1992. p. 3469–74.
[8] Gostic S, Zarnic R. Cyclic lateral response of masonry infilled RC frames and confined masonry walls. In: Proceedings of the 8th North American masonry conference, Austin; 3–6 June 1999. p. 477–88.
[9] Yanez F, Astroza M, Holmberg A, Ogaz O. Behavior of confined masonry shear walls with large openings. In: 13th World conference on earthquake engineering, Vancouver, B.C., Canada, No. 343; 2004.
[10] Lourdes Ana, Tomohisa. Evaluation of structural performance for confined masonry walls retrofitted with wire mesh and with disposable fiber mats. In: Proceedings of the 44th International Institute of Seismology and Earthquake Engineering (IISEE), Peru; 2009. p. 97–102.
[11] Flores LE, Alcocer SM. Calculated Response of confined masonry structures. In: 11th World conference on earthquake engineering, Mexico, paper No. 1830; 1996.
[12] Yoshimura K, Kikuchi K, Kuroki M, Nonaka H, Tae Kim K, Wangdi R, Oshikata A. Experimental study on effect of height of lateral forces, column reinforcement and wall reinforcement on seismic behavior of confined masonry walls. In: 13th World conference on earthquake engineering, Vancouver, Canada, No. 1597; 2004.
[13] ElGawady MA, Lestuzzi P, Bandoux M. In-plane seismic response of URM walls upgraded with FRP. J Compos Constr 2005;2005:524–35.
[14] Yu P, Silva P, Nanni A. In-plane response of URM walls strengthened with GFRP grid reinforced polyurea. In: 10th North American masonry conference, USA; 2007. p. 466–77.
[15] ASTM E519-02, 2002. Standard test method for diagonal tension (shear) in masonry assemblages.
[16] European Committee for Standardisation, EC6, Design of masonry structures. Part 1-1: general rules for buildings – rules for reinforced and un-reinforced masonry, ENV1996 1-1: Bruxels: CEN; 1995.
[17] RILEM TC: 76-LUM. Diagonal tensile strength tests of small wall specimens. In: RILEM (International Union of Laboratories and Experts in Construction Materials), recommendations for the testing and use of constructions materials, London: E&FN SPON; 1994. p. 488–89.
[18] Hose Y., Seible F. Performance evaluation database for concrete bridge components, and systems under simulated seismic loads. PEER report 1999/11, Pacific Earthquake Engineering Research Center College of Engineering, University of California, Berkley, U.S.A.; 1999.
[19] Kaushik Hemant B, Rai Durgesh C, Jain Sudhir K. Stress–strain characteristics of clay brick masonry under uniaxial compression. J Mater Civ Eng 2007;19(9):728–39. ASCE.
[20] Huang Yan, Kan Minghui, Wang Zifa. Nonlinear analysis for monotonic and low cyclic loading. Appl Mech Mater 2011;94–96:406–15.
[21] ANSYS® Academic Research, Release 12.0, ANSYS Inc.
[22] Willam KJ, Warnke ED. Constitutive model for the triaxial behavior of concrete. In: Proceedings of International Association for Bridge and Structural Engineering: seminar on concrete structures subjected to triaxial stress, ISMES, Bergamo, Italy; 1975. p. 174186.
[23] Sandeep, Renukadevi MV, Manjunath S, Somanath. Influence of reinforcement on the behavior of hollow concrete blocks masonry prism under compression – an experimental and analytical approach. Int J Res Eng Technol 2013:106–10.